@BoneJointRes

Panoramic heat map for spatial distribution of necrotic lesions

a new 3D measurement system

From The First Affiliated Hospital of Guangzhou University of Chinese Medicine, Guangzhou, China

Cite this article:
Bone Joint Res 2024;13(6):
294–305.

DOI: 10.1302/2046-3758.
136.BJR-2023-0181.R2

Correspondence should be sent to Da Guo
20182101054@stu.gzucm.edu.cn

P. Yang,[1,2,3] W. He,[4,5] W. Yang,[1] L. Jiang,[2] T. Lin,[4] W. Sun,[2] Q. Zhang,[4,5] X. Bai,[3] W. Sun,[1,2] D. Guo[1]

[1]Department of Orthopaedic Surgery, Guangdong Provincial Hospital of Chinese Medicine, Guangzhou, China
[2]Department of Orthopaedic Surgery, Shenzhen Second People's Hospital, Shenzhen, China
[3]Shenzhen Institutes of Advanced Technology, Chinese Academy of Sciences, Shenzhen, China
[4]Department of Orthopaedic Surgery, The First Affiliated Hospital of Guangzhou University of Chinese Medicine, Guangzhou, China
[5]Department of Orthopaedic Surgery, Traumatology & Orthopedics Institute of Chinese Medicine of Guangdong, Guangzhou, China

Aims
In this study, we aimed to visualize the spatial distribution characteristics of femoral head necrosis using a novel measurement method.

Methods
We retrospectively collected CT imaging data of 108 hips with non-traumatic osteonecrosis of the femoral head from 76 consecutive patients (mean age 34.3 years (SD 8.1), 56.58% male (n = 43)) in two clinical centres. The femoral head was divided into 288 standard units (based on the orientation of units within the femoral head, designated as N[Superior], S[Inferior], E[Anterior], and W[Posterior]) using a new measurement system called the longitude and latitude division system (LLDS). A computer-aided design (CAD) measurement tool was also developed to visualize the measurement of the spatial location of necrotic lesions in CT images. Two orthopaedic surgeons independently performed measurements, and the results were used to draw 2D and 3D heat maps of spatial distribution of necrotic lesions in the femoral head, and for statistical analysis.

Results
The results showed that the LLDS has high inter-rater reliability. As illustrated by the heat map, the distribution of Japanese Investigation Committee (JIC) classification type C necrotic lesions exhibited clustering characteristics, with the lesions being concentrated in the northern and eastern regions, forming a hot zone (90% probability) centred on the N4-N6E2, N3-N6E units of outer ring blocks. Statistical results showed that the distribution difference between type C2 and type C1 was most significant in the E1 and E2 units and, combined with the heat map, indicated that the spatial distribution differences at N3-N6E1 and N1-N3E2 units are crucial in understanding type C1 and C2 necrotic lesions.

Conclusion
The LLDS can be used to accurately measure the spatial location of necrotic lesions and display their distribution characteristics.

Bone & Joint Research

Article focus

- The spatial distribution of necrotic lesions impacts the outcomes following necrosis. However, the lack of effective tools for quantification and localization impedes our ability to comprehensively analyze and understand the spatial morphology of these lesions. In this study, we aimed to develop a measurement system based on computer-aided design (CAD) technology to achieve a quantitative assessment of necrotic lesions.
- The Japanese Investigation Committee (JIC) classification stands as the predominant framework employed in clinical practice, wherein type C necrosis is associated with an elevated risk of collapse. However, there is a lack of quantified data supporting the spatial distribution characteristics of type C necrosis and the differences in spatial distribution between type C1 and C2 subtypes. To bridge this gap, we intend to construct panoramic heat maps that elucidate the nuanced spatial distribution patterns inherent to distinct necrotic subtypes.

Key messages

- The longitude and latitude division system (LLDS) demonstrates good inter-rater reliability in assessing spatial distribution of necrotic lesions.
- Spatial distribution of JIC type C necrotic lesions exhibited clustering characteristics, with the lesions being concentrated in the northern and eastern regions, forming a hot zone (90% probability) centred on the N4-N6E2, N3-N6E units of outer ring blocks.
- N3-N6E1 and N1-N3E2 units may be key to the classification of the JIC type C1 and type C2.

Strengths and limitations

- A multicentre retrospective observational study was conducted, including 76 patients with non-traumatic osteonecrosis of the femoral head, comprising a total of 108 affected hips. However, this study solely focused on JIC type C1 and type C2 necrosis.
- To the best of our knowledge, this is the first investigation to depict the 2D planar and 3D spatial distribution heat map of necrotic lesions in osteonecrosis of the femoral head.
- There is a certain subjectivity in the coordinate system calibration and the judgment of necrotic lesion during the measurement process.

Introduction

Osteonecrosis of the femoral head (ONFH) is a debilitating disease arising from inadequate blood supply to the hip joint, and its pathogenesis remains unclear. The pathological process of ONFH typically progresses through three stages: necrosis, repair-collapse, and arthrosis.[1-3] The occurrence of collapse is a critical factor that determines the ultimate outcome of ONFH, as once it occurs, patients may experience severe pain and functional impairment, ultimately progressing to arthrosis.[4-9] Consequently, predicting and preventing collapse is a critical research focus in both basic and clinical research on ONFH.[10]

Medical imaging is a promising tool for predicting collapse in patients with ONFH. Several clinical studies have demonstrated that the size, location, and morphological characteristics of the necrotic lesion can influence the collapse outcome.[2,11-26] Thus, ONFH classification methods have been developed to guide clinical decision-making.[27,28] In fact, the classification methods obtained by observing the size, location, and morphology of the necrotic lesion essentially describe the spatial distribution of the necrotic lesion. However, current imaging evaluation methods suffer from low prediction accuracy and inconsistent results among various imaging methods.[29] While some studies attribute these issues to the complexity of ONFH, it is worth noting that current classification methods do not provide a comprehensive and precise description of the necrotic lesion distribution.

Here we take the Japanese Investigation Committee (JIC) classification,[30] which is the most widely used clinically, as an example. JIC classification delineates the magnitude of necrotic lesions based on anteroposterior (AP) radiograph of the hip joint, classifying them into four distinct types: JIC A, JIC B, JIC C1, and JIC C2. Notably, the type C necrosis has a heightened propensity for collapse. This classification clearly delineates the important impact of the relative position of the necrotic lesion to the weightbearing region of the femoral head on the outcome of collapse as observed on radiographs. However, the differences in the spatial distribution of the necrotic lesion among various JIC classification types remain unclear. Other classification methods, such as the Koo necrosis index method,[19] the Lafforgue method,[31] the Sugano method,[26] and the China-Japan Friendship Hospital classification method,[32] measure the necrotic lesion on a single imaging plane, and even the classification system proposed by Nishii et al[23] based on MRI measurements solely includes volumetric parameters, which are unable to provide a panoramic view of the spatial distribution of the necrotic lesion. To enable spatial measurement, a standardized measurement system is necessary. Accurately measuring the overall spatial distribution of the necrotic lesions and studying its distribution patterns can enhance understanding of necrosis subtyping or improve existing classifications. Previously, we drew upon the foundations laid by the JIC classification to formulate a predictive collapse assessment method termed the "Preserved Angle".[33] This approach integrates AP and frog-leg lateral radiographs, enabling a comprehensive quantitative evaluation of spatial morphology in necrotic lesions from diverse perspectives through radiographs. Clinical research outcomes have substantiated the simplicity and efficacy of the "Preserved Angle" as an evaluative modality. We contend that frog-leg lateral radiographs afford superior visualization of necrosis distribution on the anterior-lateral aspect of the femoral head. Although it is known that the femoral head necrotic lesion is more likely to occur in the anterior superior region,[34] the concept of "anterior superior region" is broad and vague. The specific location on the femoral head to which it refers, and the probability of occurrence, remain unclear. To elucidate this issue, it is essential to comprehensively understand the spatial distribution characteristics of necrotic lesions on the femoral head; current research on this topic is limited.

We hypothesized that the necrotic lesion exhibits varying probabilities of occurrence across different regions of the femoral head. By collecting clinical images and calculating the probability of necrosis in standardized regions, we

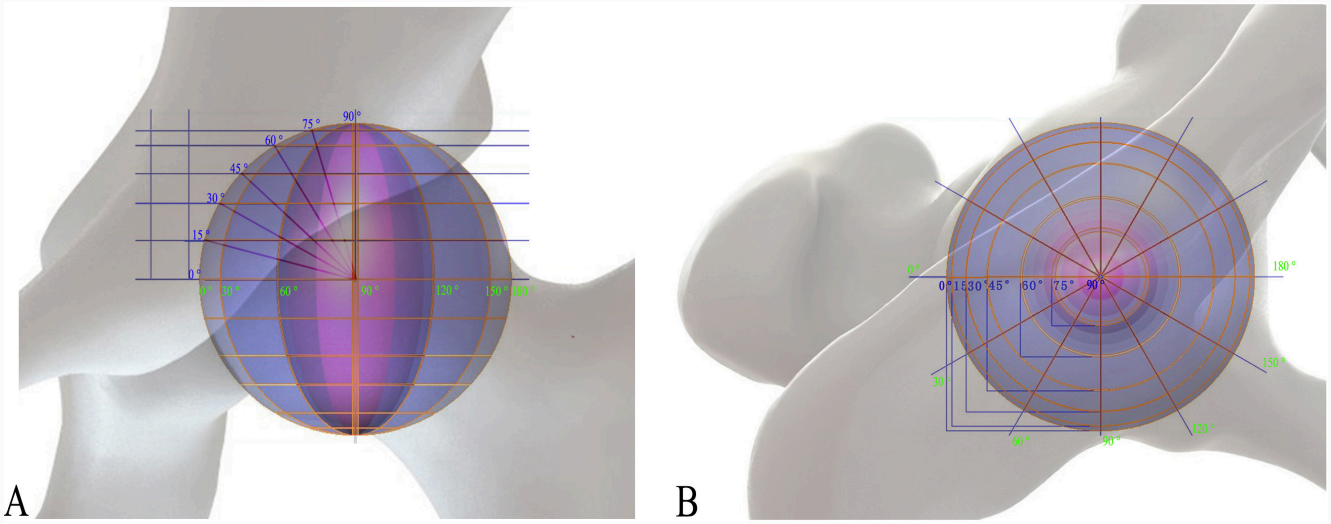

Fig. 1
Construction of the longitude and latitude division system. The brighter sphere represents the outer ring blocks, while the darker ellipsoid represents the inner ring blocks. a) Anteroposterior view. b) Top view.

can annotate and transform them into heat maps, thereby intuitively displaying the spatial distribution characteristics of the necrotic area. This study aims to address three key issues: 1) can a reference system and measurement tool for femoral head necrosis spatial measurement be developed and applied?; 2) what is the inter-rater reliability of the new measurement method?; and 3) are there differences in the spatial distribution of femoral head necrosis between JIC type C1 and type C2?

Methods

This study was conducted in accordance with the ethical standards outlined by the institutional review boards of The First Affiliated Hospital of Guangzhou University of Chinese Medicine and the Shenzhen Second People's Hospital. A retrospective analysis was conducted on CT data from 83 consecutive non-traumatic ONFH patients who were treated between September 2020 and December 2022. The medical imaging storage and transmission system of the two institutions was used to obtain CT scans with a slice thickness of ≤ 2 mm, a slice increment of ≤ 1 mm, and a pixel size of ≤ 1 mm. All patients included in the study were in stage ARCO II (no collapse) or ARCO III A (collapse less than 2 mm) according to the Association Research Circulation Osseous (ARCO) staging criteria,[35] and were classified as JIC C1 or C2 according to the JIC classification criteria,[30] owing to the elevated risk of collapse associated with these two subtypes, coupled with an ambiguity surrounding the spatial distribution distinctions between them. Seven patients were excluded as their Digital Imaging and Communications in Medicine (DICOM)-format data could not be exported, resulting in a total of 76 patients (108 hips) included in this study. All CT data from the included patients were exported in DICOM format and analyzed using Mimics software (version 16.0; Materialise, Belgium) for image processing.

The characteristics and demographics of the enrolled patients are summarized in Table I. The study population consisted of 43 males and 33 females with a mean age of 34.3 years (standard deviation (SD) 8.1). Among the 108 hips, 41 hips were classified as ARCO II and 67 hips as ARCO IIIA. There were 48 hips classified as JIC C1 and 60 hips classified as JIC C2.

Construction of spatial measurement reference system and CAD measurement tool

Unit division: a non-traumatic ONFH patient's CT data were randomly selected, and a 3D model of the ilium and proximal femur was generated using Mimics software. The resulting model was then imported into Solidworks software (version 2020; SolidWorks Corporation, USA) for assembly. The surface point cloud data of the femoral head were extracted and fitted to a sphere. To establish a spatial measurement reference system, the sphere was divided into 288 standard units using a method similar to the division of the earth's latitude and longitude (Figure 1). The 0° to 180° longitude plane was defined as the plane passing through the centre of the sphere and the axis of the femoral neck, with the outermost line being the 0° longitude. The plane passing through the centre of the sphere and perpendicular to the femoral shaft axis was defined as the equatorial plane. Using these reference planes, the sphere was first divided into 24 blocks (north and south) using planes passing through the 30°, 60°, 90°, 120°, and 150° longitudes, and then further divided into 144 blocks using planes horizontal to the 15°, 30°, 45°, 60°, and 75° latitudes. Finally, an ellipsoidal surface passing through the midpoint of the circles on each latitude plane and the 90° pole was constructed to further divide the sphere into 144 inner and outer ring blocks, totaling 288 units.

Naming convention: each unit was named according to the following rules based on the 0° longitude and latitude as reference lines (Figure 2). The 0° longitude line anticlockwise (right hip) and clockwise (left hip) 180° region was named the E region (Anterior), and the opposite was named the W region (Posterior). The upward region of the 0° latitude was named the N region (Superior), and the opposite was named the S region (Inferior). The region names of the outer and inner rings end with L and M, respectively. Using a combination

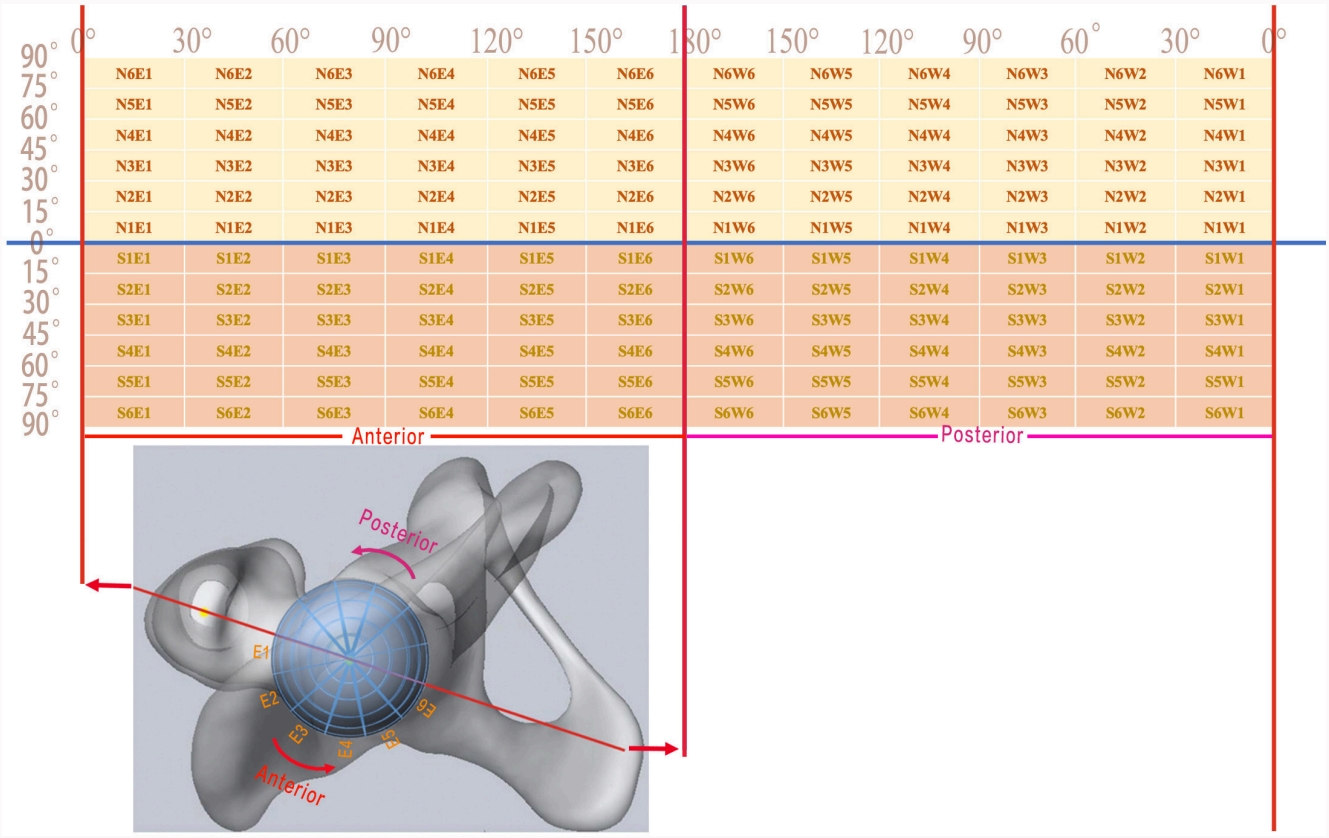

Fig. 2
Arrangement and naming rules of units (cells). Same-sized 2D cells correspond to 3D units on the sphere. The red line represents the 0° to 180° meridian, which divides the units (cells) into E[Anterior] or W[Posterior] regions, and the blue line represents the equator, which divides the units (cells) into N[Superior] or S[Inferior] regions.

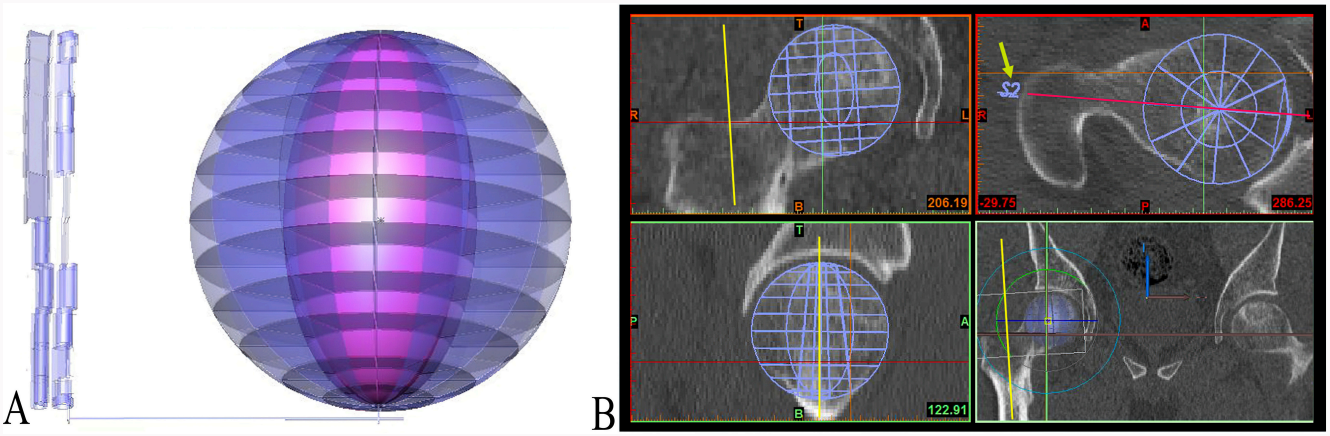

Fig. 3
Computer-aided design (CAD) measurement model and its application demonstration. a) The CAD model consists of two parts: the body and the tail. The body is composed of units, and the tail corresponds to the label of the units. b) The CAD model is registered with the femoral head on the patient's CT image. The yellow line represents the axis of the femoral shaft, while the red line represents the axis of the femoral neck. The yellow arrow indicates the label of the CAD model's tail.

of longitude and latitude, the inner and outer ring blocks, and the 288 units were named to establish a spatial structure division system based on the fitting sphere of the femoral head, known as the longitude and latitude division system (LLDS).

Based on the above division method, a standard computer-aided design (CAD) measurement model was created, including the sphere and the tail (Figure 3a). The sphere contains 288 units, and the tail contains labels corresponding to the units, enabling easy identification and measurement of the necrotic lesion location (the CAD model can be obtained through the following link: https://github.com/RYEwhiskyer/longitude-and-latitude-division-system).

Table I. The baseline characteristics and demographics of the study population.

Variable	Data (n patients = 76, n hips = 108)
Sex (M/F), n	43/33
Mean age, yrs (SD)	34.3 (8.1)
ARCO staging, n	
II	41
III A	67
JIC classification, n	
C1	48
C2	60
Associated condition, n	
Steroid-induced	29
Alcohol-associated	36
Idiopathic	11

JIC, Japanese Investigation Committee; SD, standard deviation.

Measurement of necrotic lesions

The measurement of necrotic lesions in the femoral head was performed in Mimics software using visual operations (Figure 3b). Two orthopaedic surgeons with more than five years of clinical experience (WY, LJ) were independently arranged to perform the measurements. First, the CT data of the patient were imported into Mimics, and the diameter of the femoral head displayed in the coronal intermediate plane was measured. Based on this measurement, the diameter of the standard CAD measurement model was adjusted to match the diameter of the femoral head, and then it was imported into Mimics software in STL format. The model position was adjusted to overlap with the surface of the femoral head on the coronal, sagittal, and transverse planes, and to comply with the LLDS division rules. The measurers (WY, LJ) selected the transverse view and searched layer by layer from the bottom of the femoral head upwards. The necrotic lesion was defined as the low-density area, cystic area, and sclerotic zone of the necrotic region in CT images. When a unit in the measurement model showed necrosis, it was recorded as [1], otherwise as [0]. All patient data were independently measured by the two measurers. The two independent measurement results were summarized in a 2D table containing 288 cells, with each cell recording the frequency of necrosis occurrence in its corresponding spatial unit. To better display the distribution of necrosis, the two independent measurement results were combined, and any discrepancies were re-evaluated by the third measurer (TL). The statistical frequency of each cell was converted into a percentage, and the numerical matrix of the cells was mapped into different colours to form a heat map. MATLAB software (R2017a; MathWorks, USA) was employed to construct a sphere (with a semi-axis length of [50]) and an ellipsoid (with semi-axis lengths of [3.3, 3.3, 6.2, 50]), and a command called "texture mapping" was used to warp the planar heat map onto the surfaces of the sphere and ellipsoid, thereby completing a 3D display (the programme containing the source code can be obtained through the following link: https://github.com/RYEwhiskyer/longitude-and-latitude-division-system).

Statistical analysis

For categorical variables, a proportion was used in the statistical analysis. The inter-rater reliability was evaluated using the Bland-Altman test. The differences between groups were compared using the chi-squared test. SPSS version 22 (IBM, USA) was used for the analyses. The location of the necrotic lesion was descriptive in nature. Statistical significance was set at $p < 0.05$.

Results

The inter-rater reliability

The time spent by two measurers for necrotic assessments is shown in Table II. The two independent measurement results are summarized in Figures 4a and 4b, and inter-rater reliability between two independent measurement results (N1-N6 units) was assessed by constructing a Bland-Altman plot (Figures 4c and 4d). The bias line indicates a difference of 0.153 (outer ring blocks) and 0.069 (inner ring blocks) between the means of the two variables. This indicates a strong agreement between the two measurement results, demonstrating that the new measurement system has high reliability among raters.

Spatial distribution characteristics of JIC type C necrotic lesions

A 2D heat map was generated by summarizing and calculating the results of the spatial distribution, displaying the probability of necrosis occurrence in 288 standard cells for all necrosis patients (Figures 5a and 5c). To more intuitively demonstrate the spatial distribution of necrotic lesions in the entire femoral head, a 3D heat map was formed by texture mapping on the surface of a sphere and an ellipsoid (Figures 5b and 5d), based on the 2D heat map. The colour gradient reflects the probability, with darker red indicating higher probability. As illustrated by the heat map, the distribution of necrotic lesions (JIC type C) exhibits clustering characteristics, with the lesions being concentrated in the northern and eastern regions (superior and anterior regions of the femoral head), forming a hot zone (90% probability) centred on the N4-N6E2, N3-N6E units of outer ring blocks, and N3-N6E2, N3-N6E3, N5E4 units of inner ring blocks. The heat gradually decreases in a ring gradient towards the periphery. The distributions of hot zones in the outer ring and inner ring blocks were similar, but differed slightly. The hot zones in the inner ring blocks have a larger longitude range and a smaller latitude range than those in the outer ring blocks, resulting in a slightly flattened cone-shaped distribution with a fan-shaped base on the superior anterior surface of the femoral head.

Spatial distribution characteristics of JIC type C2 and type C1 necrosis

In this section, we analyzed the distribution characteristics of necrotic lesions in 60 hips with JIC C2 and 48 hips with JIC C1. As shown by the heat maps in Figures 6 and 7, both types of necrosis exhibited clustering characteristics, with necrotic lesions concentrated in the northern and eastern regions (the superior and anterior regions of the femoral

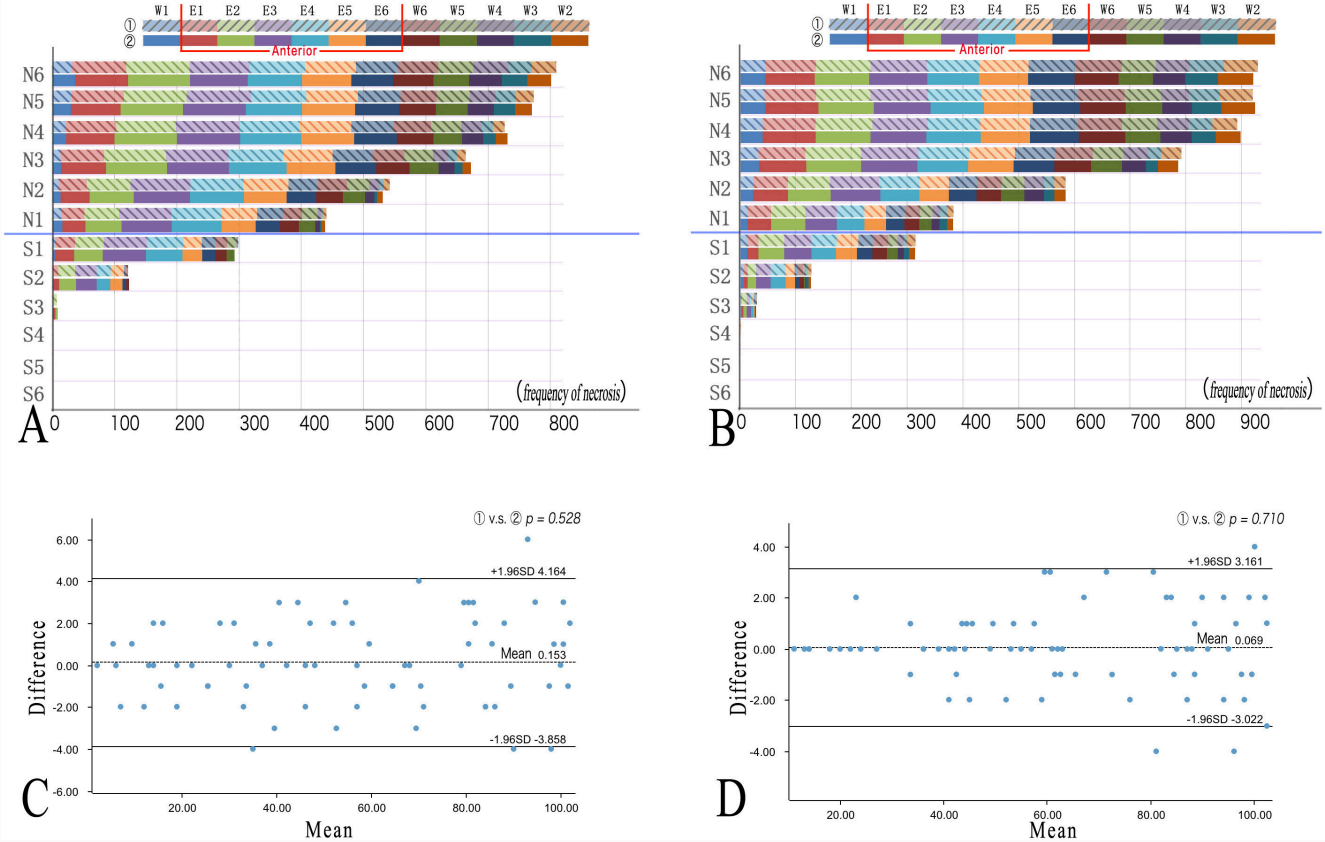

Fig. 4
Comparison of measurement results from different measurers. a) Outer ring blocks and b) inner ring blocks; the frequency of necrosis in each unit (cells) was measured by different measurers. Bland-Altman plot of two different measurement results. c) N1-N6 units of outer ring blocks and d) N1-N6 units of inner ring blocks.

Table II. A comparison of the time spent by the two measurers utilizing the longitude and latitude division system for necrotic assessments.

Measurer	Mean duration of image preparation, s (SD)	Mean duration of measure and analysis, s (SD)
No. 1	127.5 (65.3)	281.2 (98.7)
No. 2	103.0 (78.9)	316.5 (118.1)

SD, standard deviation.

head). For type C2, the hot zone (90% probability) was centred on the N3-N4E1, N2-N6E2, N2-N5E3, N4E4 units of outer ring blocks, and N3-N5E1, N3-N6E2, N3-N6E3, N4-N5E4 of inner ring blocks. The heat gradually decreased in a ring gradient towards the periphery. For type C1, the hot zone (90% probability) was centred on the N5-N6E2, N3-N6E3 units of outer ring blocks, and N5E2, N3-N6E3, N5E4 units of inner ring blocks, with the heat gradually decreasing in a ring gradient towards the periphery.

The range of hot zone for type C2 was larger than that for type C1, and the hot zone for type C2 was more offset towards the 0° longitude direction (the anterior and lateral region of the femoral head). To compare the differences in the distribution probability of necrotic lesions in the longitudinal direction (northern region) between type C2 and type C1, chi-squared test was employed (Tables III and IV). The results revealed distribution differences between type C1 and type C2 in the outer ring units E1, E2 and W1, W2, W3, as well as in the inner ring units E1, E2, and W4, W5, W6.

Discussion

The radiological evaluation of ONFH is crucial for predicting the fate of the necrotic lesion.[36] Prior research has demonstrated that the prognosis of ONFH is influenced by the size, location, and morphology of the necrotic lesion, therefore the need for a spatial description of the lesion is justified. In this study, we gathered clinical CT imaging data and employed a CAD spatial measurement technique to determine the probability of necrosis in different regions of the femoral head and explore the spatial distribution pattern of ONFH. To the best of our knowledge, this is the first investigation to illustrate the 2D planar and 3D spatial distribution heat map of necrotic lesions in ONFH.

Describing the spatial distribution of necrosis using a standardized partition of the femoral head as a sphere is a well-established research method. Malizos et al[37] devised an octants-based approach that divided the femoral head into eight regions, and assessed the spatial distribution of necrosis by quantifying the necrotic lesion volume of each octant utilizing the MRI volume method. Their study of 122 affected hips revealed that the lesion size ranged from 7% to 73% of the sphere equivalent, and the anterior superior

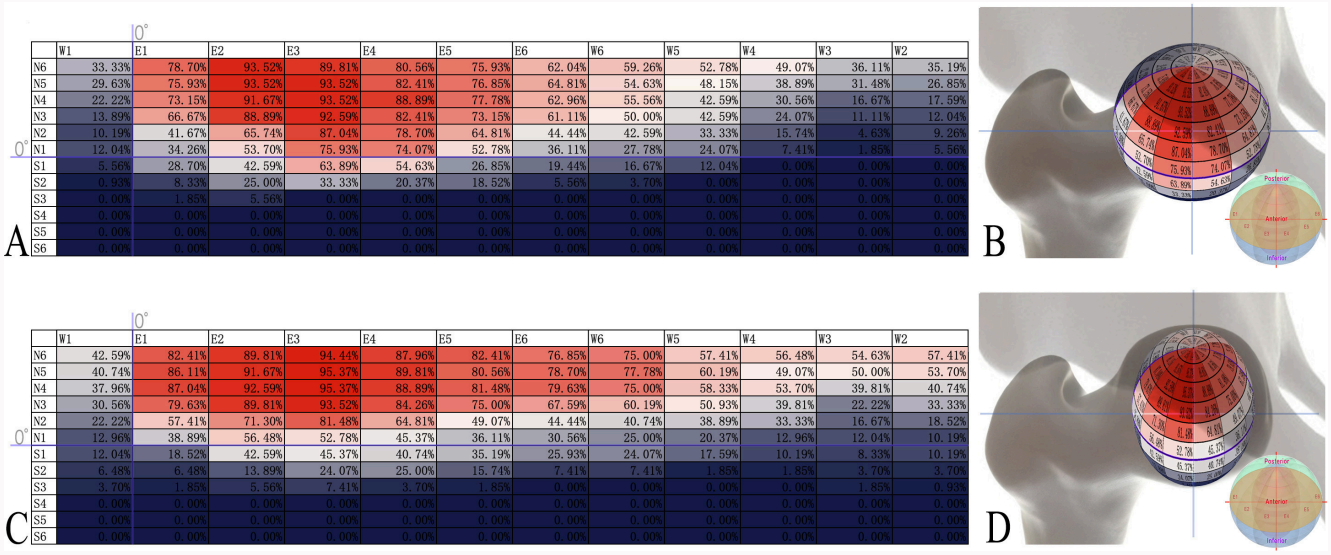

Fig. 5
Spatial distribution 2D and 3D heat maps of Japanese Investigation Committee classification type C necrosis. a) and b) Outer ring blocks. c) and d) Inner ring blocks.

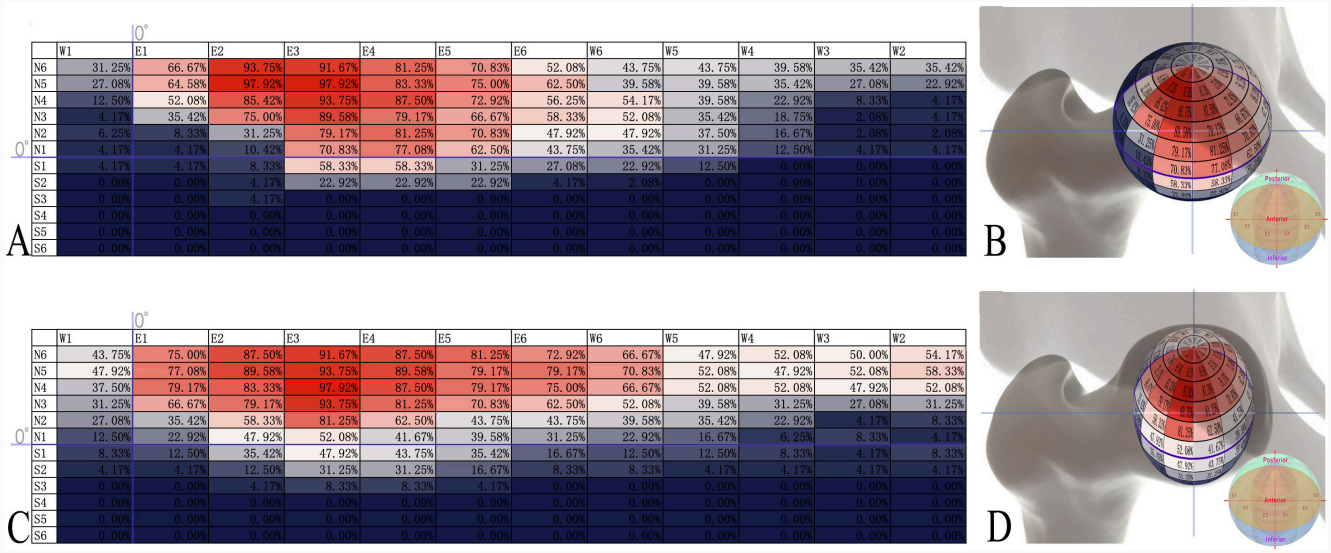

Fig. 6
Spatial distribution 2D and 3D heat maps of Japanese Investigation Committee classification type C1 necrosis. a) and b) Outer ring blocks. c) and d) Inner ring blocks.

medial octant had the largest necrotic volume. Similarly, Liu et al[38] proposed an eight-partition technique for the femoral head based on CT 3D reconstruction to examine the spatial distribution of cystic lesions in CT data of 155 ONFH patients. Their findings indicated the probability distribution of cystic lesions in different regions of the femoral head, with the anterior lateral region having the highest probability of 54%. Nevertheless, we contend that these region division methods lack sufficient accuracy to precisely locate the spatial characteristics of necrosis. The studies cited manifest certain methodological limitations in the segmentation of the femoral head. Primarily, a notable deficiency is evident in the absence of a standardized reference coordinate system and the scarcity of CAD tools capable of facilitating precise measurements. This lacuna implies the potential for measurement disparities across diverse patient cohorts. Secondly, the restricted number of delineated regions by these research methodologies impairs their ability to provide a comprehensive assessment of the spatial distribution of necrosis. Consequently, they fall short in elucidating the morphological characteristics of necrotic lesions through clustering. As a result, the generation of spatial distribution heat maps for necrotic lesions becomes an unattainable objective.

Our study possesses several distinguishing features. Firstly, we established a standardized reference system and measurement tool for spatial measurement. Standardization of the measurement reference system is a prerequisite for improving the consistency and repeatability of necrotic lesion measurement. In this study, the axis of the femoral neck and the axis of the proximal femoral shaft were selected as

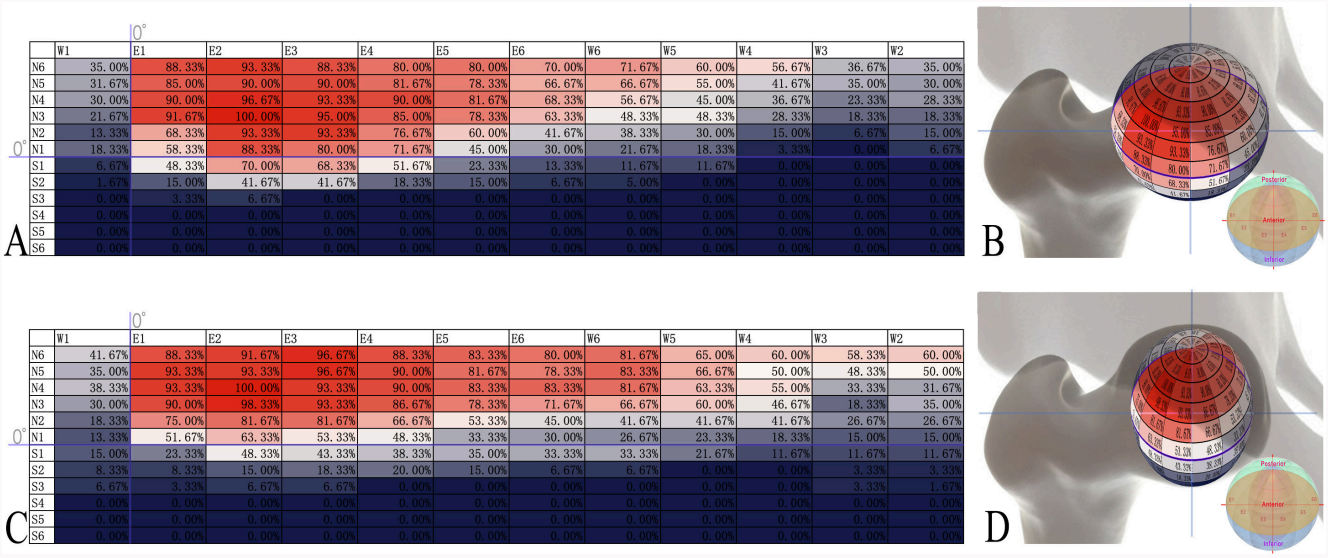

Fig. 7
Spatial distribution 2D and 3D heat maps of Japanese Investigation Committee (JIC) classification type C2 necrosis. a) and b) Outer ring blocks. c) and d) Inner ring blocks.

reference lines to construct the reference plane. This approach has the advantage of easy identification of these reference markers, and these markers are based on the femur, so measurement data are not affected by changes in patient positioning. Secondly, CAD measurement tool was used to make spatial measurement more efficient and accurate, similar to a ruler that enables the measurer to measure spatial parameters of necrosis under direct vision. The method of dividing the femoral head into 288 standard units based on the LLDS was used to quantify the spatial structure information of the necrotic lesion. The inter-rater reliability analysis showed good consistency of the measurement results, indicating the reliability of this measurement method. The method of using latitude and longitude coordinates to locate the necrosis lesion was first reported by Nishii et al[23] in 2002. However, the standard latitude and longitude positioning plane in that study was based on the coronal and sagittal planes of MRI reconstruction, which was susceptible to the influence of device scanning parameters and changes in patient positioning, and therefore lacked the reference standardization feature. Moreover, the measurement object of that study was the projection area of the quality centre of necrotic lesion on the femoral head surface, and therefore lacked the spatial standardization feature.

The present study highlights the creation of heat maps as a major feature, which depict the spatial distribution of necrotic lesions. Using the standardized units based on LLDS, we not only recorded the spatial distribution of the necrotic lesions during spatial measurement, but also noted the frequency of occurrence of necrotic lesion in each unit. This information was used to calculate the probability of occurrence of necrosis in each unit, and to generate the heat maps. A 2D heat map can swiftly show the overall distribution pattern of femoral head necrosis to observers, while a 3D heat map can display the spatial structure of necrosis on the femoral head in more detail. The heat map highlighted a marked visual contrast between the hot and cold areas of necrosis in the femoral head, indicating that there are indeed regions where necrosis occurs more frequently. Our study revealed that these regions were concentrated in the superior and anterior part of the femoral head, with the red zone (70% probability) concentrated in the range of N2-N6 and E1-E6 units, and the hot zone (90% probability) was centred on the N4-N6E2, N3-N6E units of outer ring blocks, and N3-N6E2, N3-N6E3, N5E4 units of inner ring blocks. These findings differ slightly from the reported geographical distribution of necrotic lesions by Nishii et al,[23] which may be attributed to our study including only JIC type C necrosis.

The JIC classification is widely used for predicting the risk of collapse in clinical practice.[39-41] Takashima et al[27] conducted a study to compare the accuracy of JIC classification with Steinberg classification[25] and modified Kerboul angle classification[18,19] in predicting collapse risk, and found that JIC classification was the most reliable. In addition, type C1 and type C2 necrosis were the most prevalent types of necrosis in JIC classification, accounting for 54% to 59% of cases, and had the highest risk of collapse within one year, ranging from 61% to 78%. Hence, investigating C1 and C2 necrosis is more clinically valuable. The heat map analysis revealed that the C2 necrosis hot zone (90% probability) was larger than that of C1. The C2 hot zone was also offsetting to the 0° longitude direction (anterior and lateral region of the femoral head) compared to the C1 hot zone. Statistical comparisons demonstrated significant distribution differences between type C1 and type C2 necrosis in the E1, E2 and W1, W2, W3 longitude units of outer ring blocks, and the E1, E2, and W4, W5, W6 longitude units of inner ring blocks. Combining the heat map and specific unit partitions, it was observed that the distribution differences between C1 and C2 necrosis were most pronounced in the E1 units at N3-N6 latitude level and the E2 units at N1-N3 latitude level, which are located on the anterior lateral side of the femoral head. These units could be the key units responsible for the differences in collapse risk between C1 and C2 classifications. Similarly, the hot zone

Table III. Comparison of spatial distribution of necrotic lesions between Japanese Investigation Committee classification type C1 and type C2 among different longitude units (N1-N6 units of outer ring blocks).

Region	Classification	Necrotic units/ non-necrotic units	χ^2	p-value*
	JIC C1	41/247		
W1†	JIC C2	90/270	11.49	< 0.001
	JIC C1	111/177		
E1†	JIC C2	289/71	118.0	< 0.001
	JIC C1	189/99		
E2†	JIC C2	337/23	82.0	< 0.001
	JIC C1	251/37		
E3	JIC C2	324/36	1.29	0.254
	JIC C1	235/53		
E4	JIC C2	291/69	0.06	0.805
	JIC C1	201/87		
E5	JIC C2	254/106	0.04	0.832
	JIC C1	154/134		
E6	JIC C2	204/156	0.66	0.416
	JIC C1	131/157		
W6	JIC C2	182/178	1.65	0.199
	JIC C1	109/179		
W5	JIC C2	154/206	1.61	0.204
	JIC C1	70/218		
W4	JIC C2	109/251	2.85	0.091
	JIC C1	38/250		
W3‡	JIC C2	72/288	5.26	0.021
	JIC C1	35/253		
W2†	JIC C2	80/280	11.1	< 0.001

*Chi-squared test.
†p < 0.001.
‡p < 0.05.
JIC, Japanese Investigation Committee.

Table IV. Comparison of spatial distribution between Japanese Investigation Committee classification type C1 and type C2 necrosis among different longitude units (N1-N6 units of inner ring blocks).

Region	Classification	Necrotic units/ non-necrotic units	χ^2	p-value*
	JIC C1	96/192		
W1	JIC C2	106/254	1.13	0.289
	JIC C1	171/117		
E1†	JIC C2	295/65	40.35	< 0.001
	JIC C1	214/74		
E2†	JIC C2	317/43	20.45	< 0.001
	JIC C1	245/43		
E3	JIC C2	309/51	0.08	0.784
	JIC C1	216/72		
E4	JIC C2	282/78	0.99	0.318
	JIC C1	189/99		
E5	JIC C2	248/112	0.78	0.378
	JIC C1	175/113		
E6	JIC C2	233/127	1.08	0.300
	JIC C1	153/135		
W6‡	JIC C2	229/131	7.27	0.007
	JIC C1	117/171		
W5†	JIC C2	192/168	10.36	< 0.001
	JIC C1	102/186		
W4‡	JIC C2	163/197	6.43	0.011
	JIC C1	91/197		
W3	JIC C2	120/240	0.22	0.639
	JIC C1	100/188		
W2	JIC C2	131/229	0.19	0.660

*Chi-squared test.
†p < 0.001.
‡p < 0.05.
JIC, Japanese Investigation Committee.

showed that C1 and C2 necrosis had similar distribution patterns in the E2 units at N4-N6 latitude level and the E3 units at N1-N6 latitude level on the anterior lateral side of the femoral head. These units, which had similar distribution probabilities of necrosis between C1 and C2 classifications, may be the key units responsible for a greater risk of collapse in JIC type C compared to JIC type B and type A classifications. Studies on the mechanics of ONFH have demonstrated that the anterior lateral side of the femoral head is the primary channel for stress transmission. Necrosis involving the anterior lateral side leads to greater stress concentration in the necrotic area, thereby triggering collapse.[42-45] However, the anterior lateral side is a broad concept. The current study helps to further elucidate the specific spatial localization of necrosis in the anterior lateral side and explore its impact on necrosis collapse. Our study aims to elucidate the spatial distribution disparities between type C1 and C2 necrotic lesions from a panoramic perspective, encompassing both two and three dimensions. In contrast to the JIC classification, which relies on single-view radiograph plane, the LLDS provides more precise spatial coordinates and quantitative information pertaining to necrotic lesions. This facilitates a nuanced exploration of spatial morphology within the JIC classification. The panoramic heat map results underscore significant spatial distribution variations among subtypes of type C necrosis. Investigating these distinct regions can enrich our comprehension of the nuances within the JIC classification. As previously suggested,[33] the frog-leg lateral radiographs provide a better observation of the anterior-lateral aspect of the femoral head. However, determining the localization of

these areas from frog-leg lateral radiographs will be the focus of our next step in clinical research.

However, there are some limitations in this study. Although the measurement method of spatial distribution of femoral head necrosis based on LLDS can accurately locate and measure the necrotic area with CAD measurement tool, the measurement procedure still requires a relatively long time. In actual measurement, we found that it takes a mean 6.3 (SD 1.14) minutes to measure one femoral head necrosis. A contradictory problem is that reducing the number of partitions can increase the measurement speed, but it may lead to imprecise data collection. In addition, there is a certain subjectivity in the coordinate system calibration and the judgment of necrotic lesion during the measurement process. In the future, using AI technology for semi-automatic or automatic batch measurement may be a feasible method. The challenges encompass the automatic alignment of the LLDS model with hip CT images, along with training neural networks to accomplish automatic segmentation and identification of necrotic boundaries. Leveraging these technological underpinnings, we can not only improve the measurement efficiency of the LLDS system but also achieve finer unit segmentation, thereby facilitating the acquisition of higher-resolution maps of necrotic spatial distribution. Furthermore, this study only included JIC type C necrosis, and the sample size was relatively small, so there may be selection bias. We also did not further explore the impact of spatial distribution on the outcome of necrosis collapse.

In conclusion, we proposed a novel method for measuring the spatial distribution of femoral head necrosis using CAD tool, and validated the reliability of the measurement method. We created the first 2D and 3D heat maps of the spatial distribution of JIC type C femoral head necrosis to reveal its distribution pattern, and identified the spatial distribution differences between C1 and C2 classification. These findings provide insights for more accurate imaging studies of femoral head necrosis and more precise prediction of collapse.

References

1. **Mont MA**, **Zywiel MG**, **Marker DR**, **McGrath MS**, **Delanois RE**. The natural history of untreated asymptomatic osteonecrosis of the femoral head: a systematic literature review. *J Bone Joint Surg Am*. 2010;92-A(12):2165–2170.
2. **Nishii T**, **Sugano N**, **Ohzono K**, **Sakai T**, **Haraguchi K**, **Yoshikawa H**. Progression and cessation of collapse in osteonecrosis of the femoral head. *Clin Orthop Relat Res*. 2002;400:149–157.
3. **Maestro-Paramio L**, **García-Rey E**, **Bensiamar F**, **Saldaña L**. Osteoblast function in patients with idiopathic osteonecrosis of the femoral head: implications for a possible novel therapy. *Bone Joint Res*. 2021;10(9):619–628.
4. **Im GI**. Regenerative medicine for osteonecrosis of the femoral head: present and future. *Bone Joint Res*. 2023;12(1):5–8.
5. **Chang C**, **Greenspan A**, **Gershwin ME**. The pathogenesis, diagnosis and clinical manifestations of steroid-induced osteonecrosis. *J Autoimmun*. 2020;110:102460.
6. **Fan Y**, **Zhang J**, **Chen M**, **et al**. Diagnostic value of necrotic lesion boundary in bone collapse of femoral head osteonecrosis. *Int Orthop*. 2022;46(3):423–431.
7. **Osawa Y**, **Seki T**, **Takegami Y**, **Makida K**, **Ochiai S**, **Imagama S**. Collapse progression or cessation affects the natural history of contralateral osteonecrosis of the femoral head. *J Arthroplasty*. 2021;36(12):3839–3844.
8. **Osawa Y**, **Seki T**, **Takegami Y**, **Kasai T**, **Higuchi Y**, **Ishiguro N**. Do femoral head collapse and the contralateral condition affect patient-reported quality of life and referral pain in patients with osteonecrosis of the femoral head? *Int Orthop*. 2018;42(7):1463–1468.
9. **Amin N**, **Kraft J**, **Fishlock A**, **et al**. Surgical management of symptomatic osteonecrosis and utility of core decompression of the femoral head in young people with acute lymphoblastic leukaemia recruited into UKALL 2003. *Bone Joint J*. 2021;103-B(3):589–596.
10. **Liu L-H**, **Zhang Q-Y**, **Sun W**, **Li Z-R**, **Gao F-Q**. Corticosteroid-induced osteonecrosis of the femoral head: detection, diagnosis, and treatment in earlier stages. *Chin Med J (Engl)*. 2017;130(21):2601–2607.
11. **Ansari S**, **Goyal T**, **Kalia RB**, **Paul S**, **Singh S**. Prediction of collapse in femoral head osteonecrosis: role of volumetric assessment. *Hip Int*. 2022;32(5):596–603.
12. **Kubo Y**, **Motomura G**, **Ikemura S**, **et al**. The effect of the anterior boundary of necrotic lesion on the occurrence of collapse in osteonecrosis of the femoral head. *Int Orthop*. 2018;42(7):1449–1455.
13. **Motomura G**, **Yamamoto T**, **Yamaguchi R**, **et al**. Morphological analysis of collapsed regions in osteonecrosis of the femoral head. *J Bone Joint Surg Br*. 2011;93-B(2):184–187.
14. **Wu W**, **He W**, **Wei Q-S**, **et al**. Prognostic analysis of different morphology of the necrotic-viable interface in osteonecrosis of the femoral head. *Int Orthop*. 2018;42(1):133–139.
15. **Ficat RP**. Idiopathic bone necrosis of the femoral head. Early diagnosis and treatment. *J Bone Joint Surg Br*. 1985;67-B(1):3–9.
16. **Ha Y-C**, **Jung WH**, **Kim J-R**, **Seong NH**, **Kim S-Y**, **Koo K-H**. Prediction of collapse in femoral head osteonecrosis: a modified Kerboul method with use of magnetic resonance images. *J Bone Joint Surg Am*. 2006;88 Suppl 3-A:35–40.
17. **Ito H**, **Matsuno T**, **Omizu N**, **Aoki Y**, **Minami A**. Mid-term prognosis of non-traumatic osteonecrosis of the femoral head. *J Bone Joint Surg Br*. 2003;85-B(6):796–801.
18. **Kerboul M**, **Thomine J**, **Postel M**, **Merle d'Aubigné R**. The conservative surgical treatment of idiopathic aseptic necrosis of the femoral head. *J Bone Joint Surg Br*. 1974;56-B(2):291–296.
19. **Koo KH**, **Kim R**. Quantifying the extent of osteonecrosis of the femoral head. A new method using MRI. *J Bone Joint Surg Br*. 1995;77-B(6):875–880.
20. **Min BW**, **Song KS**, **Cho CH**, **Lee SM**, **Lee KJ**. Untreated asymptomatic hips in patients with osteonecrosis of the femoral head. *Clin Orthop Relat Res*. 2008;466(5):1087–1092.
21. **Mont MA**, **Marulanda GA**, **Jones LC**, **et al**. Systematic analysis of classification systems for osteonecrosis of the femoral head. *J Bone Joint Surg Am*. 2006;88 Suppl 3-A:16–26.
22. **Nam KW**, **Kim YL**, **Yoo JJ**, **Koo KH**, **Yoon KS**, **Kim HJ**. Fate of untreated asymptomatic osteonecrosis of the femoral head. *J Bone Joint Surg Am*. 2008;90-A(3):477–484.
23. **Nishii T**, **Sugano N**, **Ohzono K**, **Sakai T**, **Sato Y**, **Yoshikawa H**. Significance of lesion size and location in the prediction of collapse of osteonecrosis of the femoral head: a new three-dimensional quantification using magnetic resonance imaging. *J Orthop Res*. 2002;20(1):130–136.
24. **Sakamoto M**, **Shimizu K**, **Iida S**, **Akita T**, **Moriya H**, **Nawata Y**. Osteonecrosis of the femoral head: a prospective study with MRI. *J Bone Joint Surg Br*. 1997;79-B(2):213–219.
25. **Steinberg ME**, **Hayken GD**, **Steinberg DR**. A quantitative system for staging avascular necrosis. *J Bone Joint Surg Br*. 1995;77-B(1):34–41.
26. **Sugano N**, **Ohzono K**, **Masuhara K**, **Takaoka K**, **Ono K**. Prognostication of osteonecrosis of the femoral head in patients with systemic lupus erythematosus by magnetic resonance imaging. *Clin Orthop Relat Res*. 1994;305:190–199.
27. **Takashima K**, **Sakai T**, **Hamada H**, **Takao M**, **Sugano N**. Which classification system is most useful for classifying osteonecrosis of the femoral head? *Clin Orthop Relat Res*. 2018;476(6):1240–1249.
28. **Sultan AA**, **Mohamed N**, **Samuel LT**, **et al**. Classification systems of hip osteonecrosis: an updated review. *Int Orthop*. 2019;43(5):1089–1095.
29. **Pierce TP**, **Jauregui JJ**, **Cherian JJ**, **Elmallah RK**, **Mont MA**. Imaging evaluation of patients with osteonecrosis of the femoral head. *Curr Rev Musculoskelet Med*. 2015;8(3):221–227.
30. **Sugano N**, **Atsumi T**, **Ohzono K**, **Kubo T**, **Hotokebuchi T**, **Takaoka K**. The 2001 revised criteria for diagnosis, classification, and staging of idiopathic osteonecrosis of the femoral head. *J Orthop Sci*. 2002;7(5):601–605.

31. **Lafforgue P**, **Chagnaud C**, **Acquaviva PC**, **Argenson JN**, **Aubaniac JM**. Quantifying osteonecrosis of the femoral head using MRI. *J Bone Joint Surg Br*. 1996;78-B(4):681–682.
32. **Liu L-H**, **Li Z-R**, **Sun W**, **Wang Y-T**, **Gao F-Q**. Reliability and repeatability of the China-Japan Friendship Hospital Typing Classification for nontraumatic osteonecrosis of the femoral head. *J Bone Joint Surg Am*. 2022;104-A(Suppl 2):40–46.
33. **Wei Q-S**, **Li Z-Q**, **Hong Z-N**, **et al**. Predicting collapse in osteonecrosis of the femoral head using a new method: preserved angles of anterior and lateral femoral head. *J Bone Joint Surg Am*. 2022;104-A(Suppl 2):47–53.
34. **Hu LB**, **Huang ZG**, **Wei HY**, **Wang W**, **Ren A**, **Xu YY**. Osteonecrosis of the femoral head: using CT, MRI and gross specimen to characterize the location, shape and size of the lesion. *Br J Radiol*. 2015;88(1046): 20140508.
35. **Yoon B-H**, **Jones LC**, **Chen C-H**, **et al**. Etiologic classification criteria of ARCO on femoral head osteonecrosis part 2: alcohol-associated osteonecrosis. *J Arthroplasty*. 2019;34(1):169–174.
36. **Pollet V**, **Bonsel J**, **Ganzeboom B**, **Sakkers R**, **Waarsing E**. Morphological variants to predict outcome of avascular necrosis in developmental dysplasia of the hip. *Bone Joint J*. 2021;103-B(5):999–1004.
37. **Malizos KN**, **Siafakas MS**, **Fotiadis DI**, **Karachalios TS**, **Soucacos PN**. An MRI-based semiautomated volumetric quantification of hip osteonecrosis. *Skeletal Radiol*. 2001;30(12):686–693.
38. **Liu G-B**, **Li R**, **Lu Q**, **et al**. Three-dimensional distribution of cystic lesions in osteonecrosis of the femoral head. *J Orthop Translat*. 2020;22:109–115.
39. **Zhao D**, **Zhang F**, **Wang B**, **et al**. Guidelines for clinical diagnosis and treatment of osteonecrosis of the femoral head in adults (2019 version). *J Orthop Translat*. 2020;21:100–110.
40. **Cheng W**, **Xian H**, **Wang L**, **et al**. Frog leg lateral view is a reliable predictor of the prognosis in osteonecrosis of the femoral head. *J Orthop Res*. 2021;39(5):950–958.
41. **Wei Q-S**, **He M-C**, **He X-M**, **et al**. Combining frog-leg lateral view may serve as a more sensitive X-ray position in monitoring collapse in osteonecrosis of the femoral head. *J Hip Preserv Surg*. 2022;9(1):10–17.
42. **Wang P**, **Wang C**, **Meng H**, **et al**. The role of structural deterioration and biomechanical changes of the necrotic lesion in collapse mechanism of osteonecrosis of the femoral head. *Orthop Surg*. 2022;14(5):831–839.
43. **Karasuyama K**, **Yamamoto T**, **Motomura G**, **Sonoda K**, **Kubo Y**, **Iwamoto Y**. The role of sclerotic changes in the starting mechanisms of collapse: a histomorphometric and FEM study on the femoral head of osteonecrosis. *Bone*. 2015;81:644–648.
44. **Wang Y**, **Yamako G**, **Okada T**, **Arakawa H**, **Nakamura Y**, **Chosa E**. Biomechanical effect of intertrochanteric curved varus osteotomy on stress reduction in femoral head osteonecrosis: a finite element analysis. *J Orthop Surg Res*. 2021;16(1):465.
45. **Wen P**, **Zhang Y**, **Hao L**, **et al**. The effect of the necrotic area on the biomechanics of the femoral head - a finite element study. *BMC Musculoskelet Disord*. 2020;21(1):211.

Author information

P. Yang, D. MD, Orthopaedic Surgeon,
Department of Orthopaedic Surgery, Guangdong Provincial Hospital of Chinese Medicine, Guangzhou, China;
Department of Orthopaedic Surgery, Shenzhen Second People's Hospital, Shenzhen, China;
Shenzhen Institutes of Advanced Technology, Chinese Academy of Sciences, Shenzhen, China.

W. He, D. MD, Orthopaedic Surgeon, Professor
Q. Zhang, MD, Orthopaedic Surgeon, Professor
Department of Orthopaedic Surgery, The First Affiliated Hospital of Guangzhou University of Chinese Medicine, Guangzhou, China; Department of Orthopaedic Surgery, Traumatology & Orthopedics Institute of Chinese Medicine of Guangdong, Guangzhou, China.

W. Yang, D. MD, Orthopaedic Surgeon, Professor
D. Guo, D. MD, Orthopaedic Surgeon, Professor
Department of Orthopaedic Surgery, Guangdong Provincial Hospital of Chinese Medicine, Guangzhou, China.

L. Jiang, MD, Orthopaedic Surgeon
W. Sun, D. MD, Orthopaedic Surgeon
Department of Orthopaedic Surgery, Shenzhen Second People's Hospital, Shenzhen, China.

T. Lin, D. MD, Orthopaedic Surgeon, Department of Orthopaedic Surgery, The First Affiliated Hospital of Guangzhou University of Chinese Medicine, Guangzhou, China.

X. Bai, D. MD, Professor, Shenzhen Institutes of Advanced Technology, Chinese Academy of Sciences, Shenzhen, China.

W. Sun, D. MD, Orthopaedic Surgeon, Professor, Department of Orthopaedic Surgery, Guangdong Provincial Hospital of Chinese Medicine, Guangzhou, China; Department of Orthopaedic Surgery, Shenzhen Second People's Hospital, Shenzhen, China.

Author contributions

P. Yang: Data curation, Methodology, Resources, Validation, Visualization, Writing – original draft, Writing – review & editing.
W. He: Data curation, Project administration, Writing – original draft, Writing – review & editing.
W. Yang: Investigation, Methodology.
L. Jiang: Investigation, Methodology.
T. Lin: Software, Validation, Visualization.
W. Sun: Formal analysis, Methodology.
Q. Zhang: Statistical analysis.
X. Bai: Conceptualization, Resources.
W. Sun: Project administration, Resources, Writing – review & editing.
D. Guo: Project administration, Supervision, Validation, Writing – review & editing.

W. Sun and D. Guo contributed equally to this work.

P. Yang and W. He are joint first authors.

Funding statement

The authors disclose receipt of the following financial or material support for the research, authorship, and/or publication of this article: D. Guo received the Guangdong Basic and Applied Basic Research Foundation (Grant No. 2021A1515011596), Guangdong Provincial Hospital of Chinese Medicine Scientific and Technological Research Special Project (Grant No. YN2020MS05), Special Research Project for Top Talents of Guangdong Provincial Hospital of Chinese Medicine (Grant No. BY2022LC06), and Science and Technology Program of Guangzhou (Grant No. 2024A03J0118). P. Yang received the Guangdong Basic and Applied Basic Research Foundation (Grant No. 2022A1515110164).

ICMJE COI statement

D. Guo received the Guangdong Basic and Applied Basic Research Foundation (Grant No. 2021A1515011596), Guangdong Provincial Hospital of Chinese Medicine Scientific and Technological Research Special Project (Grant No. YN2020MS05), Special Research Project for Top Talents of Guangdong Provincial Hospital of Chinese Medicine (Grant No. BY2022LC06), and Science and Technology Program of Guangzhou (Grant No. 2024A03J0118), all related to this study. P. Yang received the Guangdong Basic and Applied Basic Research Foundation (Grant No. 2022A1515110164), related to this study.

Data sharing

The data that support the findings for this study are available to other researchers from the corresponding author upon reasonable request.

Ethical review statement

Ethical approval for this study was obtained from the Ethical Commission of The First Affiliated Hospital of Guangzhou University of Chinese Medicine (Project ID No. k [2019]124), and the Ethical Commission of Shenzhen Second People's Hospital (Project ID 20220802012).

Open access funding

The authors report that they received open access funding for their manuscript from the Guangdong Basic and Applied Basic Research Foundation (Grant No. 2021A1515011596, Grant No. 2022A1515110164).